

## MALDI-TOF/TOF CID Study of Polystyrene Fragmentation Reactions

Anthony P. Gies,\* Matthew J. Vergne, Rebecca L. Orndorff, and David M. Hercules

Department of Chemistry, Vanderbilt University, Nashville, Tennessee 37235

Received June 4, 2007; Revised Manuscript Received July 29, 2007

**ABSTRACT:** MALDI-TOF/TOF CID experiments were conducted on a variety of hydroxylated polystyrene precursor ions ( $m/z$  1249.6 ( $n = 10$ ), 1769.9 ( $n = 15$ ), 2290.2 ( $n = 20$ ), 2810.5 ( $n = 25$ ), and 3330.8 ( $n = 30$ )) to examine the influence of molecular weight and collision kinetic energy on the degradation mechanisms. Our study indicates that polystyrene free radicals are formed initially through multiple chain breaks and subsequently undergo a variety of secondary depolymerization reactions to yield predominantly monomer, dimer, and trimer species; the intensity of each species depends on the kinetic energy selected for the CID process. Long-chain “unzipping” is not a major pathway for any of the experimental conditions. Each depolymerization mechanism is presented in detail with experimental and computational data to justify/rationalize its process and kinetic energy dependence. These processes show the complex interrelationships between the various pathways along with preferred production of secondary radicals (which suppresses the appearance of primary radicals). Additionally, Py-GC/MS experimental data are presented, for comparison of the multimolecular free radical reactions in pyrolysis with the unimolecular fragmentation reactions of MS/MS.

## Introduction

Matrix-assisted laser desorption/ionization time-of-flight mass spectrometry (MALDI-TOF MS) has proven to be an important technique for the structural and compositional analysis of synthetic polymers, allowing analysis of homo-, hetero-, and copolymers.<sup>1–3</sup> Under optimized conditions, MALDI is a soft ionization process, and as a result, MALDI mass spectra show little fragmentation.<sup>4</sup> Furthermore, through a combination of MALDI-TOF MS and collision-induced dissociation (CID) (MALDI-TOF CID), additional structural information about polymers can be determined from fragment peaks of parent ions. MALDI-TOF CID is a cumbersome process in which different mass regions (of the “post-source decay” ions) are acquired under optimized reflector potentials, and ion spectra are “sewn” together to form a composite CID spectrum. True MALDI-TOF MS/MS uses a mass spectrometer which has a collision cell between two TOF analyzers. Ions from the first TOF analyzer are filtered by a timed-ion selector, pass through a collision cell, and are accelerated into a second TOF analyzer. MS/MS allows the study of unimolecular polymer degradation (due to gas phase/low pressure dilution) in which a complete array of fragment ion masses is detected in one single, highly resolved spectrum.

Because of their commercial impact, the fraction of styrenic polymers in municipal waste facilities is increasing continuously.<sup>5</sup> Pyrolysis and gasification show great promise for the conversion of polymeric waste to more manageable materials, such as fuel or feedstocks for further chemical applications.<sup>5</sup> Thermal degradation products are of great interest to facilities involved in waste management and potential recycling of styrenic polymers. Because of this, there has been great interest in elucidating their free radical degradation mechanisms.

Traditionally, analytical pyrolysis has been employed for the analysis of polymers; applications range from product analysis and quality control to polymer longevity, degradation dynamics, and thermal stability.<sup>6</sup> The chemical reactions used to explain pyrolysis behavior of polymers are based on free radical

degradation mechanisms (initiation, propagation, and termination). Over the past 30 years numerous studies have employed Py-GC/MS to examine the effects of end groups,<sup>7</sup> molecular weight, and stereoregularity<sup>8</sup> of styrenic polymers as well as attempting to elucidate their free radical degradation mechanisms.

To date, no studies have been presented to compare data observed in the unimolecular depolymerization reactions of MS/MS and the multimolecular free radical reactions involved in pyrolysis. Given the multipath processes involved in free radical degradation, we believe such a comparison is necessary for a more complete understanding of these processes. In an effort to resolve this issue, we report the first amalgamated explanation for the multipath, free radical depolymerization of polystyrene with supporting evidence from MALDI-TOF/TOF CID and Py-GC/MS.

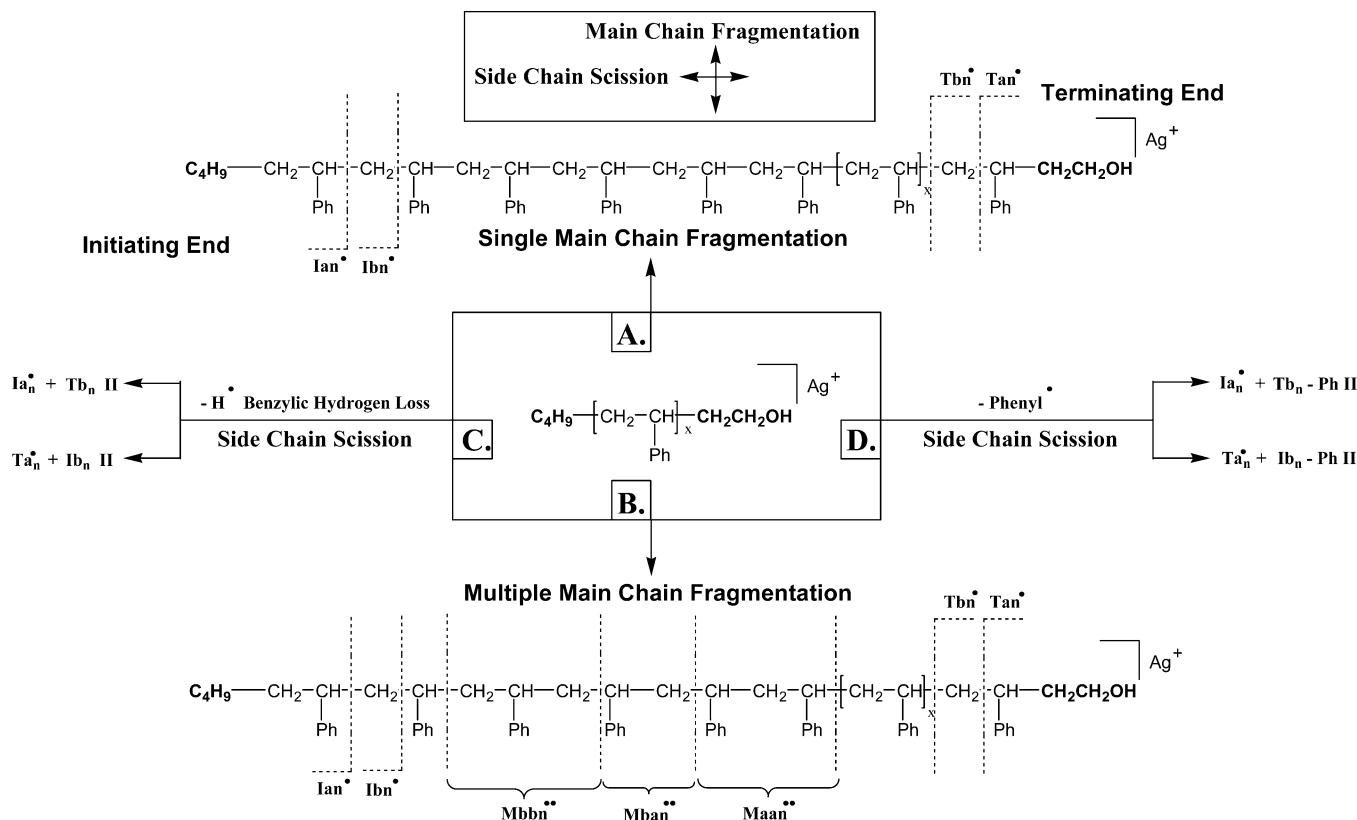
## Experimental Section

**Polystyrene Standards.** Two polystyrene standards ( $M_n = 1600$  and  $M_n = 2300$ ), synthesized by anionic polymerization, were obtained from Polymer Source, Inc. (Dorval, Canada). All samples were initiated with *sec*-butyllithium and terminated with ethylene oxide.<sup>9</sup> Their molecular weights were verified by size exclusion chromatography (SEC) and MALDI-TOF MS. The structures of the oligomers were assumed to be as shown in Scheme 1; note that they have hydroxylated end groups.

**MALDI-TOF/TOF CID Measurements.** All samples were analyzed using an Applied Biosystems 4700 Proteomics analyzer MALDI-TOF/TOF MS (Applied Biosystems, Framingham, MA) equipped with a 355 nm Nd:YAG laser. All spectra were obtained in the positive ion mode using an accelerating voltage of 8 kV for the first source and 15 kV for the second source and a laser intensity of  $\sim 10\%$  greater than threshold. The grid voltage, guide wire voltage, and delay time were optimized for each spectrum to achieve the best signal-to-noise ratio. The collision energy in the TOF/TOF instrument is defined by the potential difference between the source acceleration voltage and the floating collision cell; in our experiments this voltage difference was set to 1 kV. Air was used as a collision gas at pressures of  $1.5 \times 10^{-6}$  and  $5 \times 10^{-6}$  Torr (which will later be referred to as “low” and “high” pressure). All spectra were acquired in the reflectron mode with a mass resolution greater than 3000 fwhm; isotopic resolution was observed throughout the

\* Corresponding author: Tel (615) 343-5980; e-mail a.gies@vanderbilt.edu.

**Scheme 1. Primary CID Chemical Reactions of Hydroxylated Polystyrene: Initial (A) Single and (B) Multiple Main-Chain Bond-Breaking and/or Side-Chain (C) Hydrogen and (D) Phenyl Loss Followed by Free Radical and Even Electron Molecule Formation**



entire mass range studied. External mass calibration was performed using protein standards from a Sequazyme Peptide Mass Standard Kit (Applied Biosystems) and a three-point calibration method using Angiotensin I ( $m = 1296.69$  Da), ACTH (clip 1–17) ( $m = 2093.09$  Da), and ACTH (clip 18–39) ( $m = 2465.20$  Da). Internal mass calibration was subsequently performed using a PEG standard ( $M_n = 2000$ ; Polymer Source, Inc.) to yield monoisotopic masses exhibiting a mass accuracy better than  $\Delta m = \pm 0.1$  Da. The instrument was calibrated before every measurement to ensure constant experimental conditions. All samples were run in Dithranol (Aldrich) doped with silver trifluoroacetate (AgTFA, Aldrich) and prepared using the dried-droplet method with weight (mg) ratios of 50:10:1 (dithranol:polymer:AgTFA) in tetrahydrofuran (THF, Fisher). After vortexing the mixture for 30 s, 1  $\mu$ L of the mixture was pipetted on the MALDI sample plate and allowed to air-dry at room temperature. MS and MS/MS data were processed using the Data Explorer 4.0 software supplied by the manufacturer.

**Py-GC/MS Measurements.** All samples were analyzed using a Frontier Labs double-shot pyrolyzer (Frontier Labs, Japan) interfaced to a Hewlett-Packard 5890 II gas chromatograph and a Hewlett-Packard 5970 mass selective detector. Platinum cups were used to ensure homogeneous heating of the sample. Pyrolysis was performed using the following protocol: 0.5 mg of polymer was placed into a platinum sample cup and allowed to purge under a 100 mL/min flow of 99.999% pure (grade 5) helium for 3 min inside the upper “cool” stage of the pyrolyzer. The pyrolyzer furnace was then heated to 300 °C, the sample cupped “dropped” into the furnace, and a GC/MS was taken of the pyrolysis products. After obtaining the GC/MS, the sample cup was removed from the pyrolyzer furnace and flame-cleaned while the furnace temperature was raised 50 °C. This procedure was repeated until a temperature of 700 °C was reached by the GC/MS. The GC/MS used a heating program starting at 50 °C for 2 min and ramping at 8.0 °C/min for 31.25 min before finally holding at 300 °C for 11.75 min, for a total GC/MS heating cycle of 45 min. A 99/1 split of the carrier gas was used to ensure that the gases were introduced as a “plug” and not to corrupt the mass spectrometer.

**Bond Energy Calculations.** Models were built using GaussView 3.09. Fragmentation was simulated by homolytic bond cleavage of the parent structure. The fragments were moved  $\sim 15$  Å apart in space. Optimization was performed using the ONIOM feature of Gaussian 03 program package.<sup>10</sup> Optimization about the radical carbon was performed using DFT/B3LYP<sup>11,12</sup>/6-31G\* level of theory. The remaining portions of the fragments were optimized using DFT/B3LYP/STO-3G\* level of theory. The overall multiplicity for systems calculated with both fragments present was determined to be of triplet character. For systems independently calculated for each fragment, multiplicity was determined to be of doublet character. Following optimization, single-point energy calculations were performed, assuming a single layer for the system, using DFT/B3LYP/6-31G\* level of theory. Additional calculations were performed using DFT/B3LYP/6-31\* theory for both the triplet and doublet systems without the layering. All computations were performed in vacuo in the ground state.

## Results and Discussion

Previous polystyrene MS/MS CID fragmentation interpretations which invoke single-chain fracture and rapid monomer reversion (“unzipping”)<sup>13–15</sup> conflict with established Py-GC/MS fragmentation mechanisms which involve multiple chain breaks and a variety of interrelated degradation pathways. If long-chain unzipping is predominant, there should be a proportional increase in monomeric product ions as the molecular weight of the precursor ion increases. To test this hypothesis and to resolve the discrepancies, we conducted MALDI-TOF/TOF CID experiments on a variety of hydroxylated polystyrene precursor ions ( $m/z$  1249.6 ( $n = 10$ ), 1769.9 ( $n = 15$ ), 2290.2 ( $n = 20$ ), 2810.5 ( $n = 25$ ), and 3330.8 ( $n = 30$ )) to examine the influence of molecular weight and kinetic energy on the degradation mechanisms. The results of our studies indicate that polystyrene free radicals are initially formed through multiple chain breaks and subsequently involve a variety of depolym-

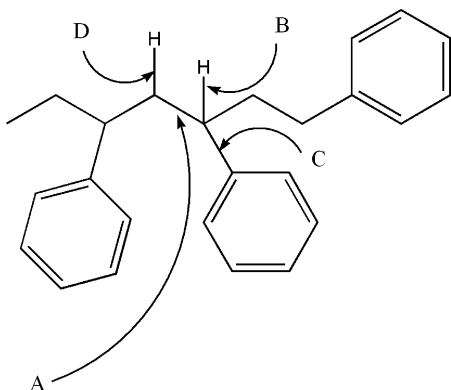


**Figure 1.** Model compound used to calculate bond-breaking energies for specified bonds.

erization side reactions (i.e., secondary reactions) to yield predominantly monomer, dimer, and trimer species. The intensity of each species depends on the kinetic energy selected in the CID process. Certain ions formed by multiple chain fracture are isobaric with ions possessing hydrogen end groups; to eliminate this problem, anionically polymerized polystyrene samples having *sec*-butyl and hydroxylated end groups were chosen for study. It is well documented that head-to-tail (H–T) propagation is the predominant (>98–99%) mode of propagation in anionic polymerization, and polystyrenes have been reported to yield no detectable head-to-head (H–H) placement.<sup>16</sup>

**Computational Results.** Because a number of bond-breaking possibilities exist for initial fragmentation of polystyrene, we performed bond energy calculations to ensure a self-consistent set of data by which we could judge the probability of a given fragmentation pathway.<sup>17</sup> In order to minimize the amount of computation time required, we selected 1,3,5-triphenylpentane as a model compound for our calculations; the structure is shown in Figure 1. Breaking bonds A through D around carbons 3 and 4 is considered to be a reasonable model for polymer fragmentation because there is a complete polymer repeat unit adjacent to either carbon. Further, the compound has an alkyl group on one end (initiator) and a hydrogen on the other (termination). Therefore, although the absolute bond energies computed may not exactly equal those in a larger styrenic polymer, their relative values should be self-consistent.

Bond energy calculations were performed using Gaussian03, following model building in GaussView3.09. The parent structure (Figure 1) was optimized using DFT/B3LYP/6-31G\* level of theory. To simulate fragmentation, a bond of interest was broken and is denoted as A, B, C, or D in Figure 1; a series of different calculation types were used to mimic homolytic cleavage. The first series of calculations involved bond cleavage followed by movement of fragments  $\sim 15$  Å apart, designated as “triplet” in Table 1. Each new bond cleavage simulation was determined to have triplet multiplicity. Additionally, each fragment was calculated independently and given doublet multiplicity, “doublet” in Table 1. This series of calculations was determined using DFT/B3LYP/6-31G\* theory.

Another set of calculations sought to determine whether the carbon radical geometry affected the energy difference between the fragments and the parent molecule. To achieve this, we layered the molecules within the calculations using the ONIOM feature of Gaussian03. Each carbon radical was optimized using DFT/B3LYP/6-31G\*, and the remainder of the molecule was optimized using DFT/B3LYP/STO-3G\* level of theory. We repeated the “triplet” and “doublet” methodology previously

described with the ONIOM layered systems representing the bond cleavages. The ONIOM calculations were designated “ONIOM layered triplet” and “ONIOM layered doublet”, respectively (Table 1). Following optimization using the ONIOM feature of Gaussian03, we performed a single-point energy calculation on the molecular fragments using DFT/B3LYP/6-31G\* to determine the energy of the fragment’s optimized state.

Overall, the theoretical bond energy values obtained from the layered calculation method (Table 1) were higher than anticipated on the basis of the available experimental bond energy data. Possibly, this is in part due to the global minimum failing to be found because of differences in the level of theory between the layers used in the calculation. Because the methodology of using different theory levels between the ONIOM layers was employed during the geometry optimization, single-point energy calculations were performed on the optimized “ONIOM layered triplet” and “ONIOM layered doublet” molecular fragments. Because of portions of the molecular fragments being optimized to various energy levels on the potential energy surface, the single-point energy calculations yielded higher bond energy values than if the fragmentation calculations had not been layered. It is also noted that the calculations designated as “triplet” in Table 1 yielded bond energy values much higher than anticipated from our obtained data (vide infra). We can conclude that this is probably the result of the triplet designation, used to simulate unpaired electrons. The values obtained from these calculations most likely reflect the energy elevation typically seen with interactions of unpaired and spin uncoupled electrons. The “doublet” calculations in Table 1, however, resulted in values very similar to those obtained from our experimental results (vide infra). The previous data from the “ONIOM layered” calculations and the “triplet” calculations further support the methodology used to arrive at the values obtained from the “doublet” calculations. The doublets determined using DFT/B3LYP/6-31G\* are representative of the minimum of each fragment upon cleavage.

**MALDI-TOF/TOF CID. Terminology.** All figures will show structures and peaks labeled according to the following key: (i) the polymer chain of origin of the species where I = initiating end group attached, T = terminating end group attached, M = main chain fragment without any end group, and Frag = a small styrenic fragment; (ii) the end group of a fragment where a = a PhCH end group and b = a CH<sub>2</sub> end group; (iii) end group modification where II = a double bond formed as a result of phenyl (Ph) or hydrogen loss; (iv) the nature of the species is indicated as free radical cation (\*) and/or silver cation (Ag<sup>+</sup>); (v) the number of repeat units (*n*) which correspond to the mass numbers found in Tables 2 and 3.

For example, a peak labeled “Ian\*Ag<sup>+</sup>” corresponds to a radical cation with a *sec*-butyl group from the initiator (I), a PhCH\* secondary radical end group (a and •), silver cationization (Ag<sup>+</sup>), and some number (*n*) of styrene repeat units. This specific example is shown at the top of Table 2. The structure of the ion is shown (minus Ag<sup>+</sup>) along with peaks observed in the TOF/TOF CID spectra for ions having different *n* values. The highest mass peak observed for a series is listed at the bottom of the series. A peak with an asterisk (e.g., \*161.1 for Ian\*) is for an ion *not* cationized with Ag<sup>+</sup>. Silver cationization of PS fragments can be verified by the distinct isotopic patterns of the peaks because of silver’s two natural isotopes (106.9 and 108.9 with a ratio of 1.00 to 0.92).

Our nomenclature, e.g., Ian\*, IanII, Maan\*, Frag 1\*, etc., for PS fragmentation differs from that used in previous MALDI CID studies (A, B, C, D, E, F, G, H, α, and β);<sup>13,14</sup> the latter

**Table 1. Calculated Atomization Values Using DFT/B3LYP/6-31G\* Level of Theory in Gaussian 03<sup>a</sup>**

calculation	A (C–C) PS backbone	B (PhC–H) benzylic H loss	C (CH–Ph) phenyl loss	D (CH–H) allylic H loss
doublet	71.87	91.66	96.21	103.69
ONIOM layered doublet	77.22	106.53	96.21	103.76
triplet	98.97	108.30	109.55	110.46
ONIOM layered triplet	77.55	107.90	100.65	108.31

<sup>a</sup> All triplet calculations were performed with the fragments  $\sim 15$  Å apart. Values are in kcal/mol.

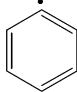
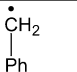
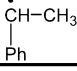
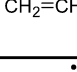
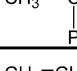
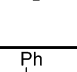
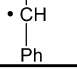
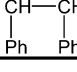
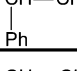
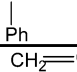
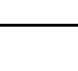
**Table 2. Structural Assignments for Peaks in the MALDI-TOF/TOF CID Mass Spectra Reported in Figures 1–3<sup>a</sup>**

Species	Structure (M)	Ag <sup>+</sup> M (Da)
<b>Ian<sup>•</sup></b> (B)	$C_4H_9-[CH_2-CH(Ph)]_x-CH_2-\dot{C}H(Ph)$ $n = 2$	*161.1 ( $n = 1$ ) 268.0 ( $n = 1$ ) 372.1 ( $n = 2$ ) 476.2 ( $n = 3$ ) 580.2 ( $n = 4$ ) 684.3 ( $n = 5$ )
<b>Ian II</b> (C)	$C_4H_9-[CH_2-CH(Ph)]_x-CH=CH(Ph)$ $n = 2$	475.2 ( $n = 3$ ) 579.2 ( $n = 4$ ) 683.3 ( $n = 5$ ) ..... 1515.8 ( $n = 13$ )
<b>Ibn II</b> (β)	$C_4H_9-[CH_2-CH(Ph)]_x-CH_2-C=CH_2(Ph)$ $n = 2$	385.1 ( $n = 2$ ) 489.2 ( $n = 3$ ) 593.2 ( $n = 4$ ) 697.3 ( $n = 5$ ) ..... 2778.5 ( $n = 25$ )
<b>Ibn – Ph II</b> (E)	$C_4H_9-[CH_2-CH(Ph)]_x-CH_2-CH=CH_2$ $n = 2$	621.3 ( $n = 5$ ) 725.3 ( $n = 6$ ) ..... 1557.8 ( $n = 14$ )
<b>Tan<sup>•</sup></b> (A)	$\dot{C}H(Ph)-CH_2-CH(Ph)-CH_2CH_2OH$ $n = 2$	*135.1 ( $n = 1$ ) 242.0 ( $n = 1$ ) 346.1 ( $n = 2$ ) 450.1 ( $n = 3$ ) 554.2 ( $n = 4$ ) 658.2 ( $n = 5$ )
<b>Tan II</b> (F)	$CH=CH(Ph)-CH(Ph)-CH_2-CH(Ph)-CH_2CH_2OH$ $n = 3$	553.2 ( $n = 4$ ) 657.2 ( $n = 5$ ) ..... 1489.7 ( $n = 13$ )
<b>Tbn II</b> (α)	$CH_2=C(Ph)-CH_2-CH(Ph)-CH_2CH_2OH$ $n = 2$	359.1 ( $n = 2$ ) 463.1 ( $n = 3$ ) 567.2 ( $n = 4$ ) 671.3 ( $n = 5$ ) ..... 2752.5 ( $n = 25$ )
<b>Tbn – Ph II</b> (D)	$H_2C=CH-CH_2-CH(Ph)-CH_2CH_2OH$ $n = 2$	595.2 ( $n = 5$ ) 699.3 ( $n = 6$ ) ..... 1531.8 ( $n = 14$ )
<b>Maan<sup>•</sup></b>	$\dot{C}H(Ph)-CH_2-CH(Ph)-H$ $n = 1$	302.0 ( $n = 1$ )
<b>Maan II</b>	$CH_2-CH_2-CH(Ph)-CH=CH(Ph)$ $n = 2$	405.1 ( $n = 2$ )
<b>Mabn II</b> (G)	$CH_2-CH_2-CH(Ph)-CH_2-C=CH_2(Ph)$ $n = 3$	211.0 ( $n = 1$ ) 315.0 ( $n = 2$ ) 419.1 ( $n = 3$ ) 523.2 ( $n = 4$ ) 627.2 ( $n = 5$ )
<b>Mbbn II</b> (H)	$CH_3-CH(Ph)-CH_2-CH(Ph)-CH_2-C=CH_2(Ph)$ $n = 3$	225.0 ( $n = 1$ ) 329.1 ( $n = 2$ ) 433.1 ( $n = 3$ ) 537.2 ( $n = 4$ )

<sup>a</sup> Underlined masses correspond to the highest mass peaks observed.

nomenclature is shown in the first column of Table 2 to allow for direct comparison. Table 2 summarizes the monoisotopic masses of the ion peak series observed in MALDI-TOF/TOF CID mass spectra from precursor polystyrene oligomer ions:  $m/z$  1249.6 ( $n = 10$ ), 1769.9 ( $n = 15$ ), 2290.2 ( $n = 20$ ), 2810.5 ( $n = 25$ ), and 3330.8 ( $n = 30$ ). All values listed are for silver-

**Table 3. Structural Assignments for Minor Fragment Peaks in the MALDI-TOF/TOF CID Mass Spectra Reported in Figures 1–3**

Species	Structure (M)	Ag <sup>+</sup> (* = no Ag <sup>+</sup> ) M (Da)
<b>Phenyl<sup>•</sup></b>	 (Ph)	* 77.0
<b>Frag 1<sup>•</sup></b>		* 91.1 198.0
<b>Frag 2<sup>•</sup></b>		* 105.1
<b>Frag 3<sup>•</sup></b>		* 117.1
<b>Frag 4<sup>•</sup></b>		* 119.1
<b>Frag 5<sup>•</sup></b>		* 131.1 238.0
<b>Frag 6<sup>•</sup></b>		* 167.1
<b>Frag 7<sup>•</sup></b>		* 181.1
<b>Frag 8<sup>•</sup></b>		* 193.1
<b>Frag 9<sup>•</sup></b>		* 207.1
<b>Frag 10<sup>•</sup></b>		253.0

cationized polystyrene fragmented under varying conditions of kinetic energy, with high ( $5 \times 10^{-6}$  Torr) and low ( $1.5 \times 10^{-6}$  Torr) pressures in the collision cell. Table 3 shows similar information for small styrenic fragment ions generated under highly energetic conditions. The ions comprising each series of peaks are separated by the mass of the polystyrene repeat unit ( $m/z$  104).

**Collision Kinetic Energy Effects on Mass Spectra.** Two experimental factors affect the collision energy for PS fragmentation at constant ion velocity: (i) the pressure in the collision cell and (ii) the molecular weight of the precursor ion. We use the following operational definitions for collision kinetic energy: (i) “High” kinetic energy will refer to the CID fragmentation of “low” molecular weight precursor ions ( $m/z = 1249.6$ ) with high pressure ( $5 \times 10^{-6}$  Torr) in the collision cell—this condition yields primarily monomeric species (e.g., Figure 2); (ii) “Medium” kinetic energy will refer to the CID fragmentation of “medium” molecular weight precursor ions



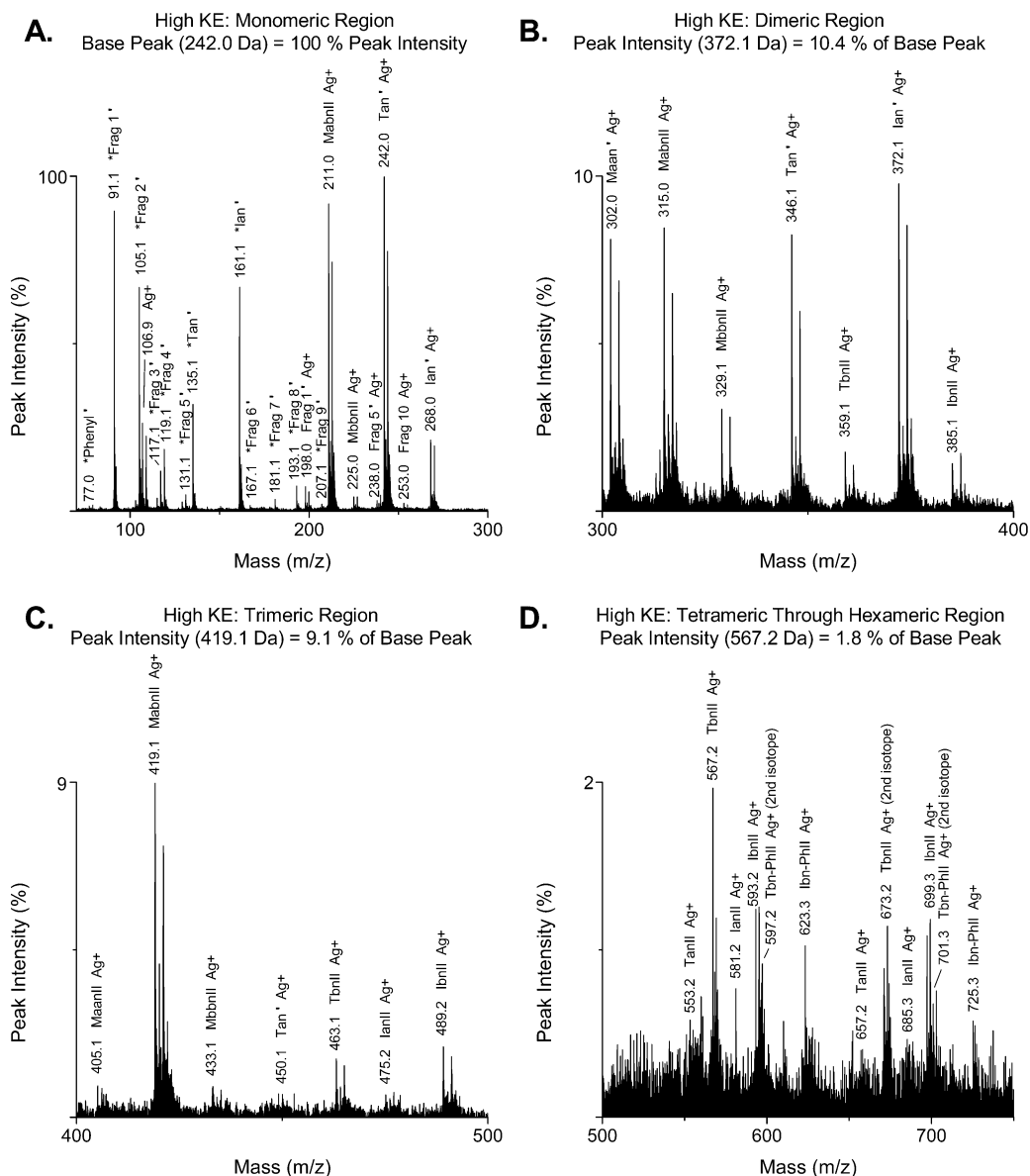


**Figure 2.** High kinetic energy (collision gas pressure:  $5 \times 10^{-6}$  Torr) MALDI-TOF/TOF mass spectrum of hydroxylated polystyrene, covering the monomeric (A: 70–300 Da), dimeric (B: 300–400 Da), trimeric (C: 400–500 Da), and tetrameric through hexameric (D: 500–750 Da) mass regions; 1249.6 Da precursor ion.

( $m/z = 1769.9$ ) with the low pressure ( $1.5 \times 10^{-6}$  Torr) in the collision cell, yielding a relatively even distribution of monomeric and dimeric species (e.g., Figure 3). (iii) “Low” kinetic energy will refer to the CID fragmentation “high” molecular weight precursor ions ( $m/z = 3330.8$ ) with low pressure ( $1.5 \times 10^{-6}$  Torr) in the collision cell which yields a relatively even distribution of dimeric and trimeric species (e.g., Figure 4). The rationale for this nomenclature is that ions in the high-pressure mode will undergo more collisions and that higher molecular weight ions will be better able to dissipate collision energy internally without fragmentation.

**Overview of Bond-Breaking Reactions.** Three different types of reactions can produce ions in the CID of polystyrene. First, initial breaking of C–C bonds in the polymer chain will lead to main-chain fragments, e.g., Ian<sup>+</sup>, Tan<sup>+</sup>, Ibn<sup>+</sup>, and Tbn<sup>+</sup>. Second, multiple fracture of the polymer chain can lead to distonic radical ions, e.g., Maan<sup>•</sup>, Mabn<sup>•</sup>, and Mbn<sup>•</sup>. These processes are shown in Scheme 1 by the arrows from “A” and “B”, respectively. A third possibility is initial loss of either a benzylic hydrogen atom or a phenyl group with subsequent main-chain fracture which produces both free radicals and even-electron

molecules, e.g., IbnII, TbnII, Ibn-PhII, and Tbn-PhII. These processes are shown in Scheme 1 by the arrows from “C” and “D”, respectively.

Free radicals produced by initial bond-breaking reactions can subsequently undergo reactions secondary to initial C–C bond cleavage. Because we are dealing with molecules in the gas phase at very low pressures, these are considered to be unimolecular reactions. Charge on nearly all of the fragments is provided by Ag<sup>+</sup> attachment, presumably to a phenyl group. Because of the similarities between our MS/MS fragmentation (with silver cationization) and Py-GC/MS (without silver cationization), we consider that MS/MS fragmentation occurs remote from the charge site.<sup>6</sup> To ensure that this assumption is reasonable, we carried out calculations using the same parameters as the doublet calculations in Table 1 for the molecule shown in Figure 1 but cationized (with Na<sup>+</sup>) on the middle phenyl ring. The question was whether the bond labeled “A” (C4–C5) would differ from the adjacent C–C bond (C3–C4) for the cationized species. The two calculated bond energies were essentially identical: C3–C4 = 74.62 kcal/mol and C4–C5 = 74.72 kcal/mol. These differ little from the C–C bond

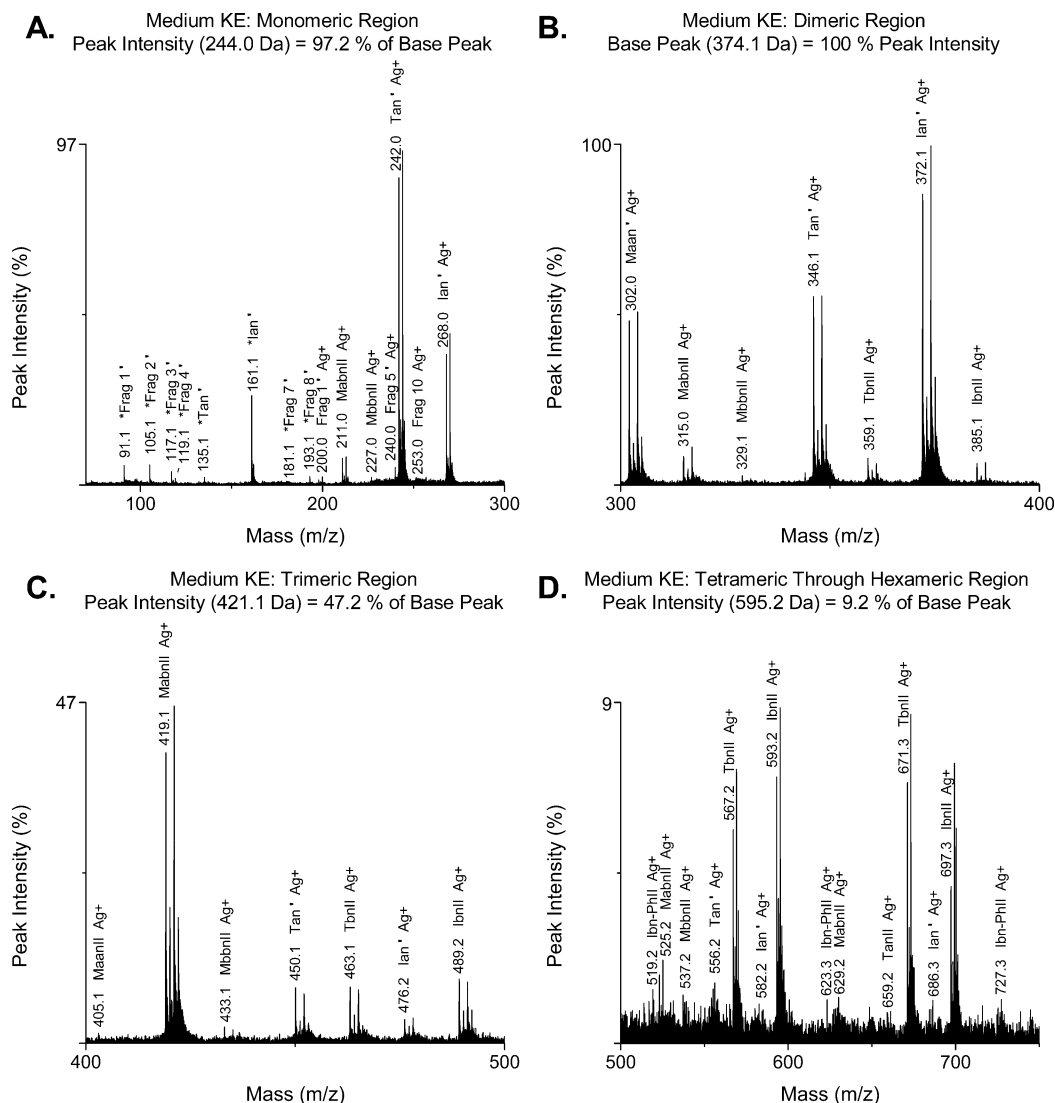


**Figure 3.** Medium kinetic energy (collision gas pressure:  $1.5 \times 10^{-6}$  Torr) MALDI-TOF/TOF mass spectrum of hydroxylated polystyrene, covering the monomeric (A: 70–300 Da), dimeric (B: 300–400 Da), trimeric (C: 400–500 Da), and tetrameric through hexameric (D: 500–750 Da) mass regions; 1769.9 Da precursor ion.

energies for bond A calculated in Table 1. Thus, it seems to be unlikely that there is preferential radical formation at the carbon attached to the cationized phenyl group.

Schemes 2–5 show the complex interrelationships between the various fragmentation pathways along with preferred production of secondary radicals; each mechanism will be discussed in greater detail below. Earlier studies<sup>13,14</sup> proposed that polystyrene fragment ions were formed solely through single chain fragmentation followed by hydrogen rearrangement and  $\beta$ -scission reactions similar to mechanisms proposed for PS field desorption mass spectra. However, our MALDI-TOF/TOF CID mass spectra (Figures 2–4) and Py-GC/MS pyrograms (Figure 5) indicate that there is a strong correlation between collision kinetic energy and the degree of chain fragmentation.

Multiple bond-breaking reactions dominate under high-energy CID conditions. For example, in Figure 2 the most intense peaks are in the mass range characteristic of low molecular weight monomeric species (70–300 Da). The peaks above 300 Da are only 10% the intensity of the lower mass peaks at best. The base peak in the spectrum of Figure 2 is at 242.0 Da and is due to Tan<sup>•</sup>,  $n = 1$ . Other significant peaks are from MabnII,  $n = 1$  (211.0); \*Frag 1<sup>•</sup> (91.1); \*Frag 2<sup>•</sup> (105.1); and \*Ian<sup>•</sup>,  $n = 1$

(161.1). Contrast this with the spectrum taken under low-energy conditions shown in Figure 4. The most intense peaks are observed in the mass range 300–500 Da which are characteristic of dimeric and trimeric species. Peaks below 200 Da (monomeric region) are virtually absent. The base peak at 372.1 is from Ian<sup>•</sup>,  $n = 2$ . Other significant peaks in the dimeric region are from Tan<sup>•</sup>,  $n = 2$  (346.1), and Maan<sup>•</sup>,  $n = 2$  (302.0); in the trimeric region the predominant peaks are (MabnII,  $n = 3$  (419.1, 421.1), Tan<sup>•</sup>,  $n = 3$  (450.1), TbnII,  $n = 3$  (463.1), Ian<sup>•</sup>,  $n = 3$  (476.2), and IbnII,  $n = 3$  (489.2).

Also, *long-chain* monomer reversion (chain “unzipping”) is not observed under any of the experimental conditions, but *short-chain* monomer reversion is, as shown in Scheme 2. This interpretation parallels polymer fragmentation reactions observed for secondary-ion mass spectra (SIMS); such studies have been reported for polystyrenes as well as many other homopolymers.<sup>18</sup> The analogy with SIMS is probably better than with field desorption because SIMS and MALDI-CID both involve highly energetic collisions. Even though the initial ion impact in SIMS is very energetic (5–10 keV), it has been shown that SIMS fragmentation is consistent with interpretation by thermal bond-breaking reactions.<sup>18</sup> Also, many of the reactions proposed here have been used to explain the pyrolysis of polystyrene.<sup>19</sup> Clearly,

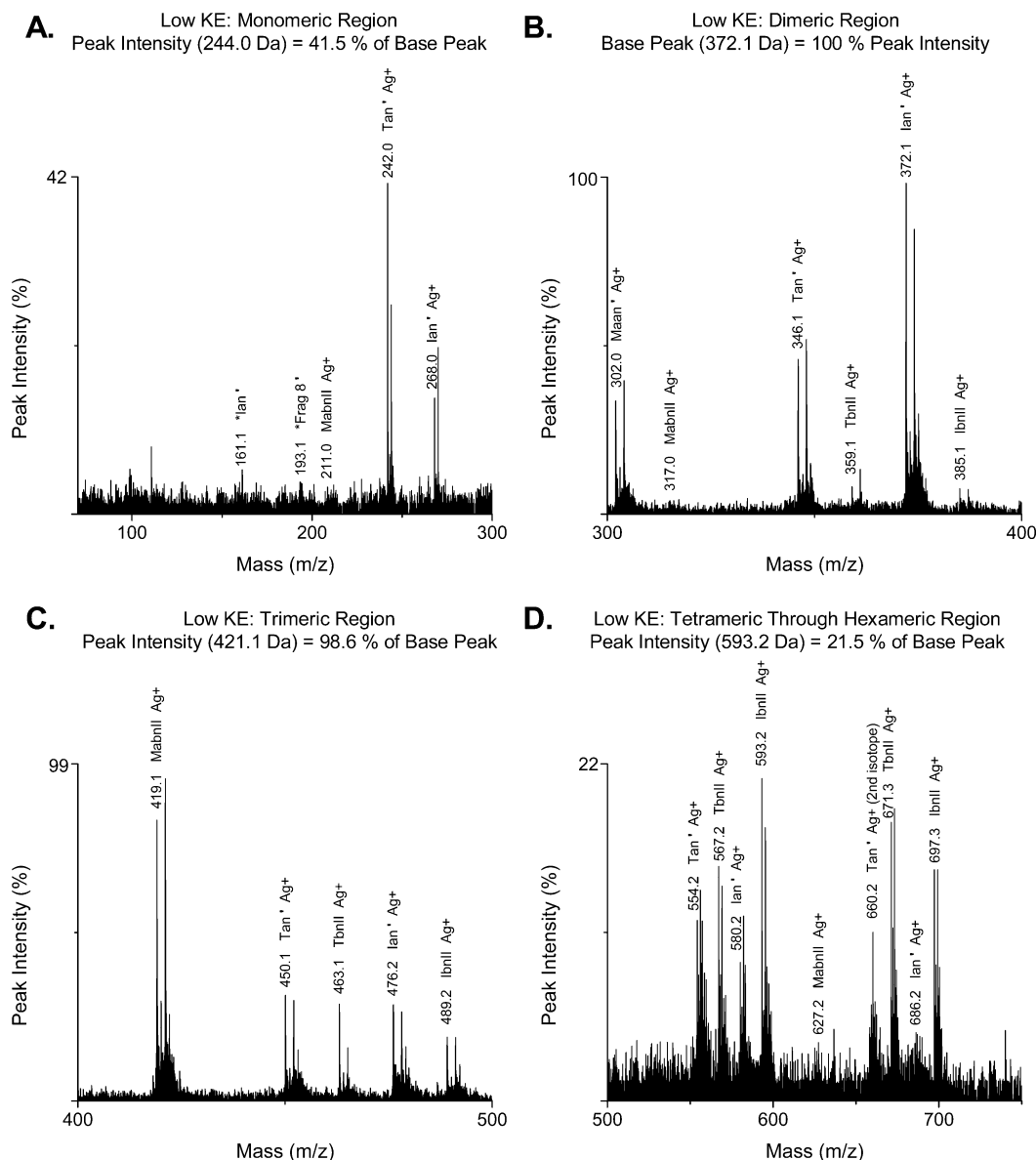
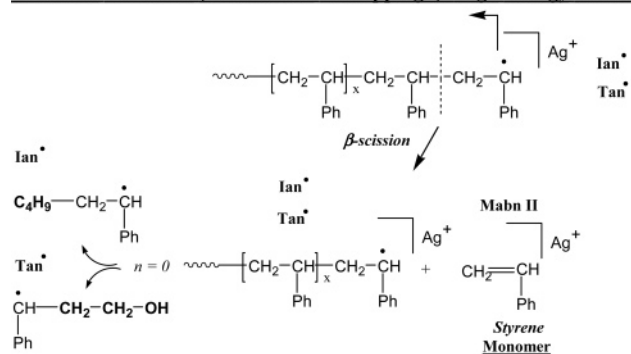


**Figure 4.** Low kinetic energy (collision gas pressure:  $1.5 \times 10^{-6}$  Torr) MALDI-TOF/TOF mass spectrum of hydroxylated polystyrene, covering the monomeric (A: 70–300 Da), dimeric (B: 300–400 Da), trimeric (C: 400–500 Da), and tetrameric through hexameric (D: 500–750 Da) mass regions; 3330.8 Da precursor ion.

**Scheme 2. Monomer Reversion (Short-Chain Unzipping):  
Major Secondary Chemical Reaction Pathway of Polystyrene  
Secondary Radicals**

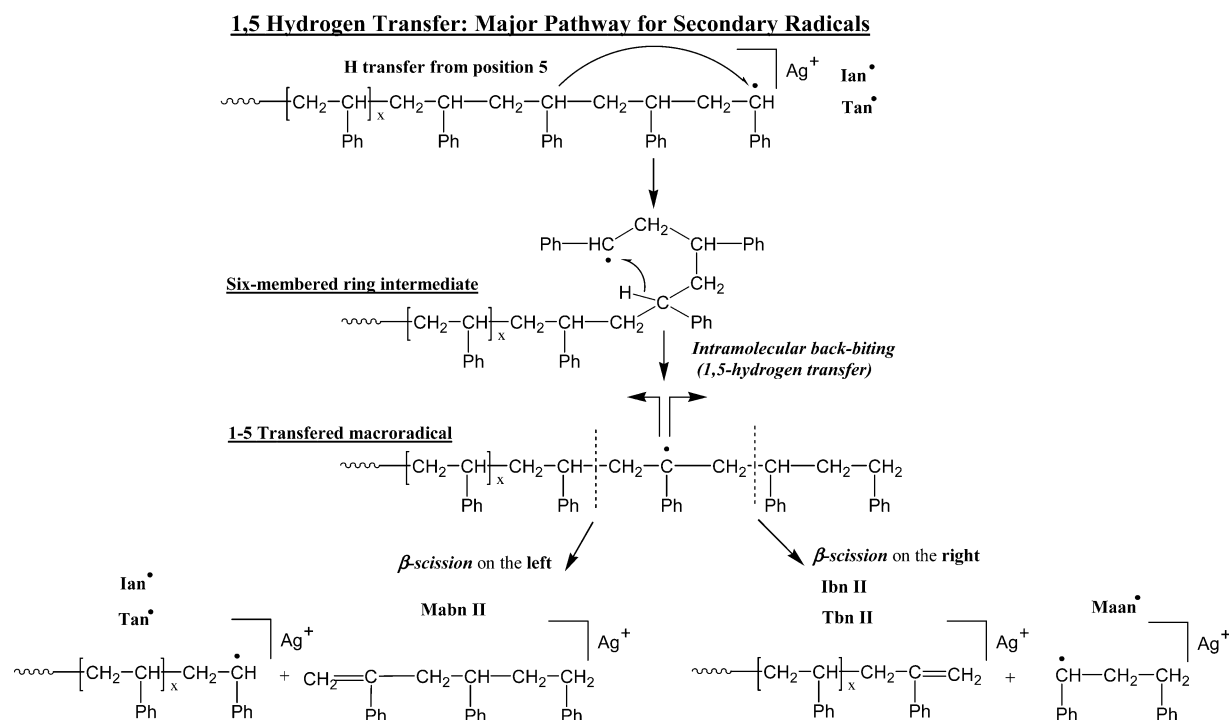
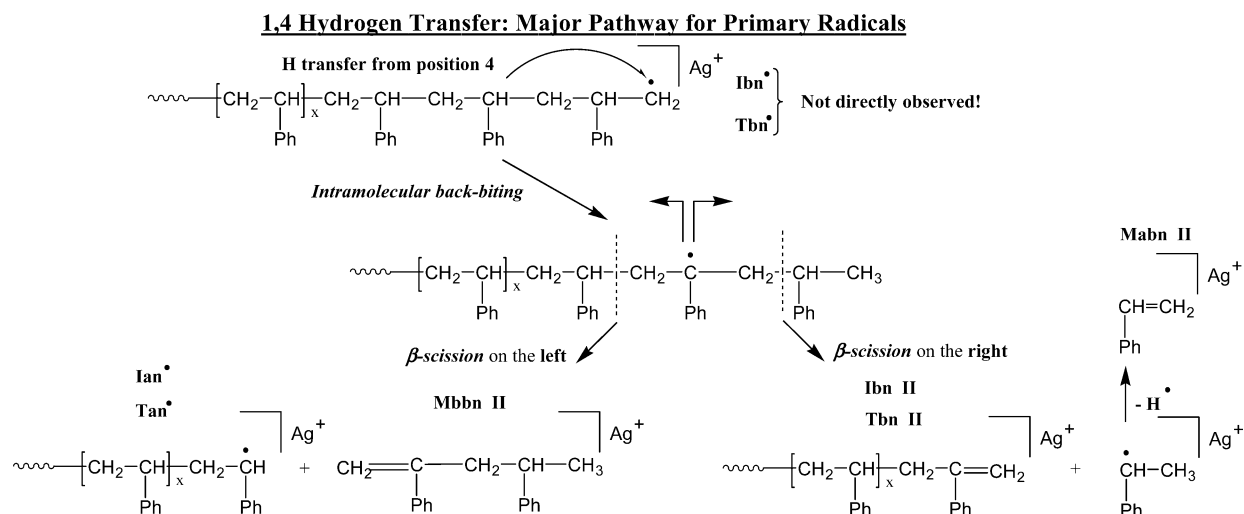
**Monomer Reversion (Short-Chain "Unzipping"): High Energy Pathway**



such reactions involve thermal energies. Next we will consider the initial chain cleavage reactions first and provide experimental data to support the explanations given above.

**Initial Bond-Breaking Reactions.** Pathways A and B in Scheme 1 show the possible origins of the Ian\*, Ibn\*, Tan\*, Tbn\*,

Maan\*\*, Mabn\*\*, and Mbn\*\* series, all of which result from single- or multiple main-chain cleavage reactions. The energy of the main-chain C–C bond (A in Figure 1) is computed to be 71.87 kcal/mol and is the lowest-energy bond in polystyrene; thus, it will be the most likely bond to break. This also means that most of the secondary reactions will involve radicals formed by cleavage of the main-chain C–C bond. Pathways C and D in Scheme 1 show alternative processes for initial free radical formation through benzylic hydrogen or phenyl group loss followed by chain cleavage. The computed bond energies for benzylic hydrogen (B in Figure 1) and phenyl group (C in Figure 1) loss are 91.66 and 96.21 kcal/mol, respectively; they will compete to some extent for initial radical formation. No lines are observed in the spectra for the ions formed initially in these processes (e.g., loss of H• or Ph•), but species produced by  $\beta$ -scission of the initial ions are prominent. For example, in pathway D of Scheme 1,  $\beta$ -scission to the left or right after phenyl loss produces Ian\* and Tan\* radicals along with Ibn-PhII and Tbn-PhII even-electron species. Benzylic hydrogen loss followed by  $\beta$ -scission to the left or right produces

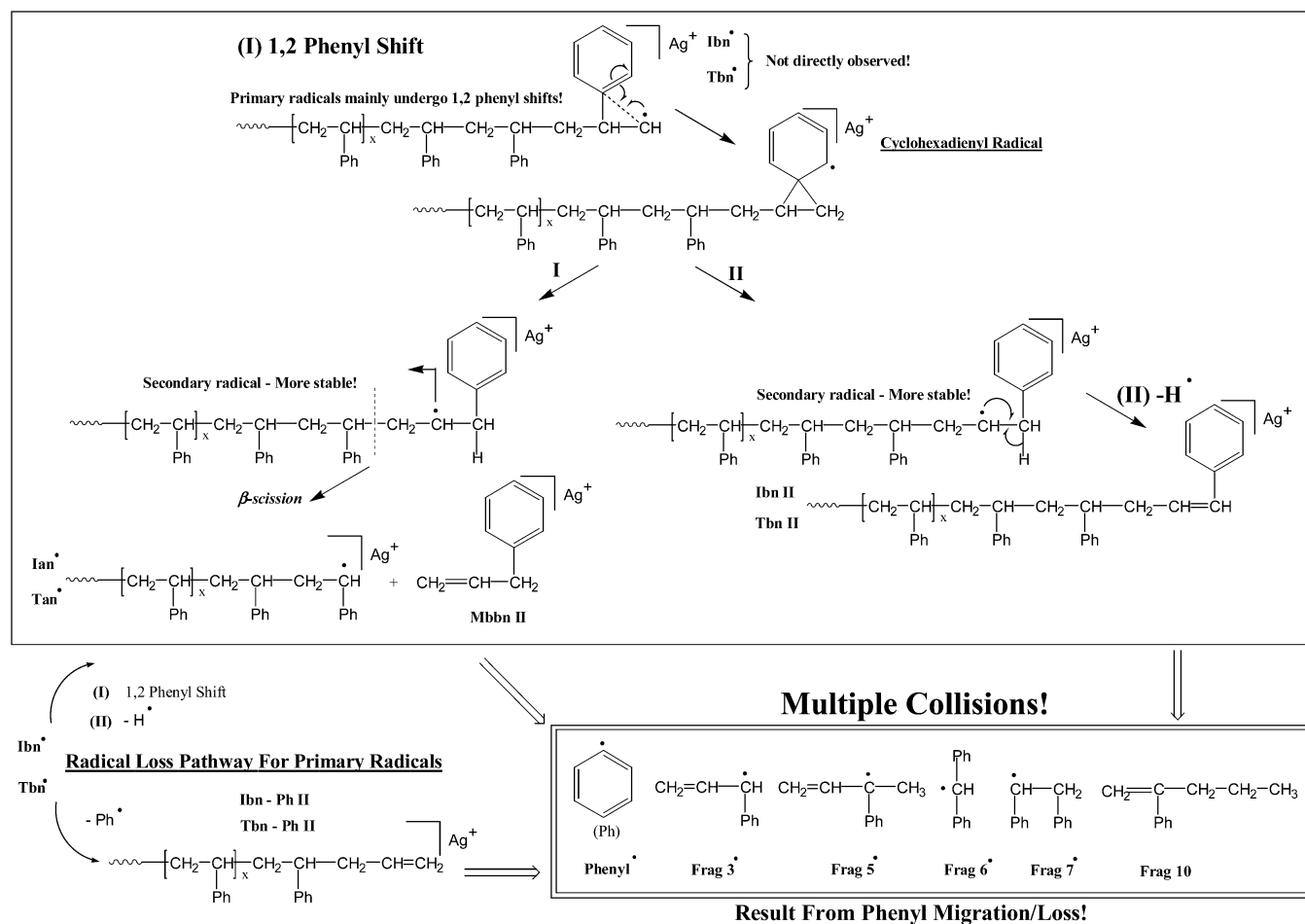
Scheme 3. 1,5-Hydrogen Transfer Followed by  $\beta$ -Scission: Major Secondary Chemical Reaction Pathway of Polystyrene Secondary RadicalsScheme 4. 1,4-Hydrogen Transfer Followed by  $\beta$ -Scission: Major Secondary Chemical Reaction Pathway of Polystyrene Primary Radicals

Ian $\cdot$  and Tan $\cdot$  radicals along with IbnII and TbnII species (pathway C).

Initial phenyl group loss is most pronounced for high-energy conditions, consistent with relative bond energies. The high mass series begin with Tbn-PhII ( $n = 5$ ) at 595.2 Da (Figure 2D) and Ibn-PhII ( $n = 5$ ) at 621.3 Da and continue to 1115.5 Da ( $n = 14$ ) and 1557.8 Da ( $n = 14$ ) for Tbn-PhII and Ibn-PhII, respectively. The absolute intensities are very low relative to those from monomeric species (Figure 2A). The phenyl ion at 77.0 Da is observed (Figure 2A) under high-energy conditions (although it is weak) but is absent for other conditions. Under medium kinetic energy conditions (Figure 3D) peaks for the Tbn-PhII and Ibn-PhII series are weak but still visible. Under low kinetic energy conditions (Figure 4D), no tetrameric through hexameric fragment ions are observed from initial phenyl group loss. These results are consistent with the order of bond-breaking calculated in Table 1. The highest energy bond corresponds to phenyl group loss.

Peaks corresponding to initial loss of benzylic hydrogen are seen more consistently than those for phenyl group loss; both TbnII and IbnII are readily observed under high-energy conditions. Figure 2D shows TbnII ( $n = 4$ ) at 567.2 Da and IbnII ( $n = 4$ ) at 593.2 Da which continue to 2752.5 Da ( $n = 25$ ) and 2778.5 Da, respectively. More intense peaks from lower members of both series are seen in the dimeric (Figure 2B) and trimeric (Figure 2C) regions. Under medium kinetic energy conditions (Figure 3D), peaks corresponding to benzylic hydrogen loss account for the major peaks observed in the tetrameric through hexameric mass range, although still weak relative to monomeric and dimeric species; TbnII and IbnII dominate this region. Under low kinetic energy conditions (Figure 4D), peaks due to TbnII and IbnII have intensities about 20% of the base peak. It seems unlikely that the small energy difference between the benzylic C-H bond and the C-Ph bond (4.5 kcal/mol) can account for this discrepancy in intensity changes. As will be seen (vide infra), the TbnII and IbnII species



**Scheme 5. Phenyl and Hydrogen Loss (with 1,2-Phenyl Shift): Minor Secondary Chemical Reaction Pathway of Polystyrene Primary Radicals**

can arise from secondary reactions as well as primary C–H bond scission, the former playing a significant role.

**Secondary Bond-Breaking Reactions of Secondary Radicals. Monomer Reversion.** Initial chain fragmentation produces Ian<sup>•</sup>, Ibn<sup>•</sup>, Tan<sup>•</sup>, and Tbn<sup>•</sup> radicals as shown by pathway A in Scheme 1. Any of these primary radicals can, in principle, undergo monomer reversion, namely direct loss of styrene monomer as shown in Scheme 2. A similar argument holds for Maan<sup>•</sup>, Mabn<sup>•</sup>, and Mbbn<sup>•</sup>, secondary radicals formed by multiple chain fragmentation (pathway B in Scheme 1). Repeated iterations through the reversion cycle by loss of styrene molecules is referred to as “chain unzipping”. If monomer reversion were the dominant pathway for primary radical degradation, one would expect that peaks at 104.0 Da for the styrene radical and 211.0 Da for the silver cationized styrene monomer would dominate the spectrum obtained under high-energy conditions. Figure 2A clearly reveals that this is not the case. No peak is observed at 104.0 Da; the peak at 211.0 Da is strong, but no stronger than that for \*Frag 1<sup>•</sup> at 91.1 Da and Tan<sup>•</sup> at 242.0 Da.

Multiple chain-breaking under high-energy conditions is emphasized by the production of monomeric fragment peaks in Figure 2A such as 91.1 (\*Frag 1<sup>•</sup>), 105.1 (\*Frag 2<sup>•</sup>), and to a lesser extent 119.1 (\*Frag 3<sup>•</sup>). Other monomeric species observed are 135.1 Da (\*Tan<sup>•</sup>), 161.1 Da (\*Ian<sup>•</sup>), 242.0 Da (Tan<sup>•</sup>), and 268.0 Da (\*Ian<sup>•</sup>, *n* = 1). Even for fragmentation using medium kinetic energy (Figure 3A), there are some peaks resulting from chain breaking followed by monomer reversion. However, the majority of the monomeric species observed

probably result from multiple chain breaking not involving monomer reversion. Under low kinetic energy conditions (Figure 4A), monomer reversion is essentially nonexistent due to the insufficient energy necessary for this pathway. Therefore, the monomeric species observed at 211.0 (MabnII, *n* = 1), 242.0 (Tan<sup>•</sup>, *n* = 1), 161.1 (\*Ian<sup>•</sup>, *n* = 1), and 268.0 (Ian<sup>•</sup>, *n* = 1) are the result of multiple chain breaking. If long-chain monomer reversion were predominant, then as the molecular weight of the precursor ion increased, there should be a proportional increase in monomeric product ions; the opposite is observed in our spectra, supporting multiple bond-breaking in the polymer backbone.

**1,5-Hydrogen Transfer Followed by  $\beta$ -Scission.** Scheme 3 shows a major fragmentation pathway for the allylic Ian<sup>•</sup> and Tan<sup>•</sup> radicals produced by initial chain fragmentation. The major pathway is 1,5-hydrogen transfer (“backbiting”), and an accompanying minor pathway is 1,3-hydrogen transfer. After formation of the 1,5-macroradical,  $\beta$ -scission to the left produces smaller Ian<sup>•</sup> and Tan<sup>•</sup> radicals which can continue this depolymerization pathway or can undergo monomer reversion (Scheme 2). Neutral MabnII species are also produced accounting for peaks at 419.1 Da for 1,5-H transfer and 315.0 Da for 1,3-H transfer.  $\beta$ -Scission to the right produces IbnII and TbnII species which give series starting at 385.1 Da (*n* = 2) and 359.1 Da (*n* = 2), respectively, along with the Maan<sup>•</sup> species at 302.0 Da for 1,5-H transfer and 198.0 Da for 1,3-H transfer; a peak from Frag 1<sup>•</sup> at 91.1 Da (no silver cationization) is also observed.

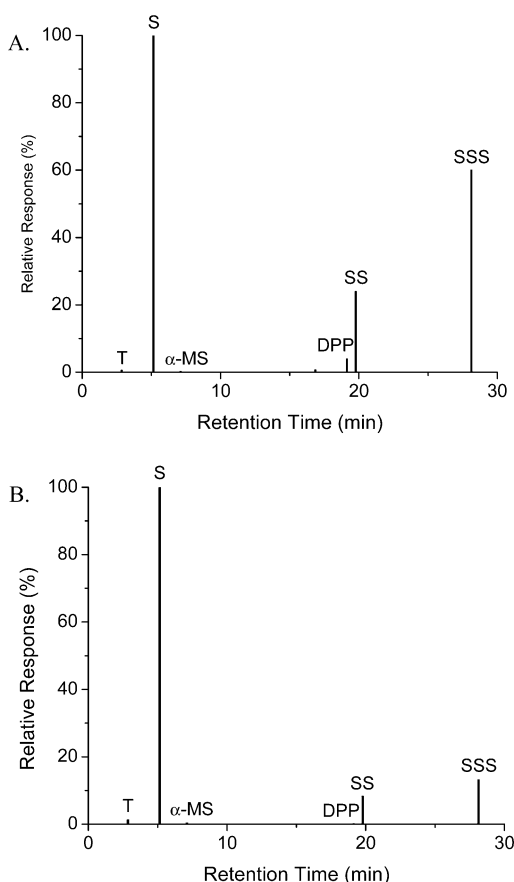


**Figure 5.** Py-GC/MS representative programs of 0.5 mg polystyrene ((A)  $M_n = 3500$  and (B)  $M_n = 75\,000$ ) at  $500\text{ }^{\circ}\text{C}$ . The following fragments were observed: T (toluene), S (styrene monomer),  $\alpha$ -MS ( $\alpha$ -methylstyrene), DPP (1,3-diphenylpropane), SS (styrene dimer), and SSS (styrene trimer).

Under high-energy fragmentation conditions (Figure 2A,B), the peaks due to hydrogen transfer followed by  $\beta$ -scission are weak relative to those from small monomeric species, indicating that hydrogen transfer is a secondary pathway. 1,5-Hydrogen transfer with  $\beta$ -scission to the right gives Maan\* at  $302.0\text{ Da}$  ( $n = 2$ ), and  $\beta$ -scission to the left gives for MabnII at  $419.1\text{ Da}$  ( $n = 3$ ). These are highly favored over 1,3-hydrogen transfer with  $\beta$ -scission right giving  $198.0\text{ Da}$  (Frag 2\*) and  $\beta$ -scission left giving  $315.0\text{ Da}$  MabnII ( $n = 2$ ). It should be noted that the  $\beta$ -scission right and left produces peaks of equal intensity since, statistically, both scissions are equally favorable. Compare  $302.0$  and  $419.1\text{ Da}$  in Figure 2.

Under medium kinetic energy conditions (Figure 3), multiple chain-breaking is preferred; however, the production of dimeric peaks is predominant with monomeric fragment peaks being secondary. For example, the peaks from hydrogen transfer followed by  $\beta$ -scission, Maan ( $n = 2$ ) at  $302.0\text{ Da}$  and MabnII ( $n = 3$ ) at  $419.1\text{ Da}$ , have intensities about 50% of base peak. This can be explained by hydrogen transfer followed by  $\beta$ -scission requiring less energy vs monomer reversion (a higher energy pathway). Secondary radicals, again, prefer 1,5-hydrogen transfer relative to 1,3-hydrogen transfer; compare peaks from Frag 2 at  $198\text{ Da}$  and MabnII ( $n = 2$ ) at  $315\text{ Da}$  with the intensities of the  $302.0$  and  $419.1$  peaks. It should be noted that  $\beta$ -scission right or left produces peaks of equal intensity since both scissions are equally favorable.

Under low kinetic energy conditions (Figure 4), multiple chain-breaking is still observed; however, the production of dimeric and trimeric peaks is predominant along with consider-

able production of tetrameric through hexameric species. For example, for the IbnII and TbnII species having  $n = 4$  and  $n = 5$  the intensities have increased to about 20% of the base peak. Monomer reversion is essentially nonexistent because of insufficient energy to propagate this pathway. 1,5-Hydrogen transfer is very significant; the  $302.0$  and  $419.1\text{ Da}$  peaks have intensities in the range 50–100% of base peak. 1,3-Hydrogen transfer is not observed. Because  $\beta$ -scission right and left should produce peaks of equal intensity, the exaggerated  $419.1$  peak intensity is probably from multiple chain-breaking and minor ion production from 1,5-hydrogen transfer.

**1,4-Hydrogen Transfer Followed by  $\beta$ -Scission.** Scheme 4 shows another fragmentation pathway for the primary radicals Ibn\* and Tbn\* resulting from initial chain fragmentation; 1,4-hydrogen transfer is the major route while 1,2- and 1,6-hydrogen transfer are minor.  $\beta$ -Scission of the 1,4-macroradical to the left produces Ian\* and Tan\* radicals which can react according to the Scheme 5 depolymerization pathway or undergo monomer reversion. The MbbnII species gives peaks at  $329.1\text{ Da}$  for 1,4-H transfer,  $225.0\text{ Da}$  for 1,2-H transfer, and  $433.1\text{ Da}$  for 1,6-H transfer.  $\beta$ -Scission to the right produces IbnII and TbnII species along with MabnII species, the latter at  $211.0\text{ Da}$  for 1,4-H transfer and  $315.0\text{ Da}$  for 1,6-H transfer.

Under high-energy conditions (Figure 2), a small amount of 1,4-hydrogen transfer followed by  $\beta$ -scission is also observed for primary radicals.  $\beta$ -Scission to the left produces a peak for MbbnII that is quite weak, about 3% of the base peak. The peaks for IbnII and TbnII are similarly weak, about 1–2% each. The peak intensities for 1,2- and 1,6-hydrogen transfer reactions are even weaker. Once again,  $\beta$ -scission to the right or left should produce peaks of equal intensity, so it is clear that the  $211.0$  peak intensity comes from other reactions, most likely monomer reversion. Under medium kinetic energy conditions (Figure 3), 1,4-hydrogen transfer followed by  $\beta$ -scission either to the right or left gives peaks that are weak relative to the base peak but more intense than under high-energy conditions; however, more intense than those for 1,2- or 1,6-hydrogen transfer reactions. Once again,  $\beta$ -scission right or left should produce peaks of equal intensity; therefore, the contribution to the  $211.0$  peak is predominantly from 1,4-hydrogen transfer and is minimal from monomer reversion. Secondary radicals (Ian\* and Tan\*) are still prominent in the tetrameric through hexameric mass region Under low kinetic energy conditions (Figure 4), 1,4-hydrogen transfer followed by  $\beta$ -scission is not observed for primary radicals, indicating that it is a higher energy pathway that is optimized under medium-energy conditions.

**1,2-Phenyl Shift and Phenyl Loss.** Scheme 5 shows additional fragmentation pathways for primary radicals (Ibn\* and Tbn\*) resulting from the initial chain fragmentation, a 1,2-phenyl shift followed by hydrogen loss which is a major pathway under low-energy fragmentation conditions (Figure 4) and phenyl group loss which is a major pathway under high-energy fragmentation conditions (Figure 2). These two processes account for minor peaks in all of the monomeric regions, but for pronounced peaks in the tetrameric through hexameric regions.

The 1,2-phenyl shift in the initial radical, followed by hydrogen loss, results in IbnII and TbnII species and phenyl loss results in Ibn-PhII and Tbn-PhII species. Peaks characteristic of all four species are evident under high-energy conditions, for example, the peaks at  $623.3$  and  $597.2\text{ Da}$  in Figure 2D. They are quite weak, being only about 1% of the base peak. They appear at about the same relative intensity for medium-energy conditions and are completely absent for low-energy

conditions (Figure 4D). This correlates with phenyl group loss being a high-energy pathway.

Behavior of peaks for a 1,2-phenyl shift followed by hydrogen loss (IbnII and TbnII) is entirely different. They appear weakly under high-energy conditions (<2% of base peak), increase in intensity for medium-energy conditions (ca. 9% of base peak), and show significant intensity for low-energy conditions, ca. 20% of the base peak. The combination of the well-known phenyl shift reaction<sup>20,21</sup> coupled with loss of hydrogen to form a stable olefin represents a lower-energy pathway for polymer decomposition.

Other peaks are apparent under high kinetic energy conditions (Figure 2A): low mass fragment ions at  $m/z$  117.1 (\*Frag 3\*), 131.1 (\*Frag 5\*), 167.1 (\*Frag 6\*), 181.1 (\*Frag 7\*), 238.0 (Frag 5\*), and 253.0 (Frag 10). They disappear under other conditions, indicating a high-energy pathway for their formation. It is quite likely that some of these are derived from high-energy fragmentation of either the initially formed radical or one of the intermediate species in Scheme 5.

**Py-GC/MS.** An important question is whether studies of the decomposition of isolated free radicals in the gas phase, such as the present one, can provide any insights into the mechanism(s) of pyrolysis in the condensed phase. If we assume that the initial chain-breaking reactions are the same for both types of studies, then it seems that studies such as the present one are highly relevant.

The temperature at which thermal decomposition of polystyrene begins is 300–330 °C<sup>20</sup> and starts with multiple chain-breaking (i.e., initiation), followed by depropagation, hydrogen/phenyl abstraction, and (in some cases) termination steps. Under “very high” kinetic energy conditions (500 °C and above), styrene, the most abundant product from polystyrene degradation, is reportedly produced primarily by monomer reversion (depropagation though  $\beta$ -scission of polystyrene radicals, Scheme 2). Figure 5 shows that polymers with higher molecular mass (Figure 5B) give a higher yield of monomer (styrene (S):  $m/z$  = 104, ret time = 5.15 min) compared to those of lower molecular mass (Figure 5A).<sup>20</sup> However, significant amounts of other products are produced and include toluene (T:  $m/z$  = 92),  $\alpha$ -methylstyrene ( $\alpha$ -MS:  $m/z$  = 118), 1,3-diphenylpropane (DPP:  $m/z$  = 196), styrene dimer (SS: 2,4-diphenyl-1-butene) ( $m/z$  = 208), and styrene trimer (SSS: 2,4,6-triphenyl-1-hexene) ( $m/z$  = 312).

Consistent with the literature, the highest molecular weight compounds identified in our study by gas chromatography were those with three phenyl substituents (SSS), and only trace quantities of benzene, tetramer, pentamer, etc., were detected in the gaseous products.<sup>22</sup> However, it should be noted that Py-GC/MS condensed phase final products, from very high kinetic energy conditions (500 °C), do yield proportional increases in monomeric species (styrene (S):  $m/z$  = 104) with increases in polymer molecular weight. This observation would appear to support the hypothesis of the predominance of long-chain unzipping to yield, sequentially, multiple styrene molecules. However, on the basis of our collision kinetic energy studies with isolated gas phase precursor ions, we conclude that the increase of monomeric species (styrene, S) with increased polymer molecular weight is primarily the result of multiple main-chain-breaking (Scheme 1A) followed by short-chain monomer reversion (Scheme 2), i.e., loss of only a few styrenes.

Additionally, our gas phase CID studies have identified the preferential formation of secondary radicals which under go hydrogen transfer and  $\beta$ -scission reactions (Scheme 3). The major pathway is 1,5-hydrogen transfer followed by  $\beta$ -scission

left, producing smaller secondary radicals along with MabnII trimer species (2,4,6-triphenyl-1-hexene, SSS), or right, producing IbnII and TbnII species along with Maan\* species which can abstract a hydrogen in the condensed phase to yield 1,3-diphenylpropane (DPP). The minor pathway is 1,3-hydrogen transfer followed by  $\beta$ -scission left to give smaller secondary radicals along with MabnII trimer species (2,4-diphenyl-1-butene, SS), or right to give IbnII and TbnII species along with Maan\* species which can abstract a hydrogen in the condensed phase to yield toluene (T). It should be noted that the  $\beta$ -scission right or left should produce peaks of equal intensity since, statistically, both scissions are equally favorable. Therefore, by inspection of the intensities of peaks T and DPP, we can conclude that the exaggerated dimer (SS) and trimer (SSS) peaks are primarily the result of monomer recombination in the condensed phase, with a minor contribution from gas phase hydrogen transfers followed by  $\beta$ -scission in the preferentially formed secondary radicals.

## Conclusions

The combination of MALDI-TOF/TOF CID and Py-GC/MS was successfully exploited to examine the fragmentation reactions of functionalized polystyrene. Findings indicate that (1) free radicals are initially formed through multiple chain breaks and subsequently go through a variety of secondary reactions, (2) fragment ion peak intensities differ vastly depending on the kinetic energy conditions utilized in fragmentation, and (3) the interrelationship multipath, free radical degradation processes (along with phenyl migration) favor the production of secondary radicals and suppresses the appearance of primary radicals in the mass spectra. We believe our studies are the first to provide documented correlation between unimolecular MS/MS studies and multimolecular Py-GC/MS polystyrene fragmentation reactions.

**Acknowledgment.** We thank William K. Nonidez for use of his Py-GC/MS instrument and Ned Porter and Piotr Kaszyiski for helpful discussions.

## References and Notes

- Hanton, S. D. *Chem. Rev.* **2001**, *101*, 527.
- White, T. P.; Dolan, A. R.; Maziarz, E. P.; Wood, T. D. In *Comprehensive Desk Reference of Polymer Characterization and Analysis*; Brady, R. F., Ed.; Oxford University Press: Oxford, 2003; p 248.
- Pasch, H.; Schrepp, W. *MALDI-TOF Mass Spectrometry of Synthetic Polymers*; Springer-Verlag: Berlin, 2003.
- Montaudou, G.; Montaudou, M. S.; Samperi, F. In *Mass Spectrometry of Polymers*; Montaudou, G., Lattimer, R. P., Eds.; CRC Press: Boca Raton, FL, 2002; p 419.
- Faravelli, T.; Pinciroli, M.; Pisano, F.; Bozzano, G.; Dente, M.; Ranzi, E. *J. Anal. Appl. Pyrol.* **2001**, *60*, 103–121.
- Wampler, T. P. *Applied Pyrolysis Handbook*; Marcel Dekker: New York, 1995.
- Ohtani, H.; Ueda, S.; Tsukahara, Y.; Watanabe, C.; Tsuge, S. *J. Anal. Appl. Pyrol.* **1993**, *25*, 1–10.
- Nonobe, T.; Ohtani, H.; Usami, T.; Mori, T.; Fukumori, H.; Hirata, Y.; Tsuge, S. *J. Anal. Appl. Pyrol.* **1995**, *121*, 121–138.
- Quirk, R. P.; Ma, J.-J. *J. Polym. Sci., Part A: Polym. Chem.* **1988**, *26*, 2031–2037.
- Frisch, M. J.; et al. Gaussian, Inc., Wallingford, 2004.
- Becke, A. D. *Phys. Rev. A* **1988**, *38*, 3098.
- Lee, C.; Yang, W.; Parr, R. G. *Phys. Rev. B* **1988**, *38*, 3098.
- Scrivens, J. H.; Jackson, A. T.; Yates, H. T.; Green, M. R.; Critchley, G.; Brown, J.; Bateman, R. H.; Bowers, M. T.; Gidden, J. *Int. J. Mass Spectrom. Ion Processes* **1997**, *165/166*, 363–375.
- Scrivens, J. H.; Jackson, A. T. *Int. J. Mass Spectrom.* **2000**, *200*, 261–276.
- Pastor, S. J.; Wilkins, C. L. *Int. J. Mass Spectrom. Ion Processes* **1998**, *175*, 81–92.

- (16) Odian, G. *Principles of Polymerization*, 4th ed.; John Wiley & Sons: Hoboken, NJ, 2004.
- (17) Stoliarov, S. I.; Westmoreland, P. R. *Polymer* **2003**, *44*, 5469.
- (18) Hercules, D. M. In *Mass Spectrometry of Polymers*; Montaudo, G., Lattimer, R. P., Eds.; CRC Press: Boca Raton, FL, 2002; pp 311–388.
- (19) Tsuge, S.; Ohtani, H. In *Mass Spectrometry of Polymers*; Montaudo, G., Lattimer, R. P., Eds.; CRC Press: Boca Raton, FL, 2002; pp 113–147.
- (20) Moldoveanu, S. C. *Analytical Pyrolysis of Synthetic Organic Polymers*; Elsevier: New York, 2005.
- (21) Nonhebel, D. C.; Walton, J. C. *Free-Radical Chemistry*; Cambridge University Press: London, 1974.
- (22) Woo, O. S.; Kruse, T. M.; Broadbelt, L. J. *Polym. Degrad. Stab.* **2000**, *70*, 155–160.

MA0712450